

Development of Selective Inhibition Sintering (SIS) for Metallic Parts Fabrication

Mahdi Yoozbashizadeh, Behrokh Khoshnevis

Daniel J. Epstein Department of Industrial and Systems Engineering,

University of Southern California, Los Angeles CA, 90089,

Email: yoozbash@usc.edu; khoshnev@usc.edu

Nozar Mozaka

Quality Engineer, JE Pistons, Inc., 15312 Connector Lane, Huntington Beach, CA 92649, USA,

Email: nmozaka@gmail.com

Abstract: *The SIS-Metal process based on microscopic mechanical inhibition is a layer-based rapid prototyping process. In the process, salt solution is printed in the selected area of each metal powder layer; the salt re-crystallizes when water evaporates; salt crystals decompose and grow rapidly prior to sintering; the generated decomposed salt particles spread between metal powder particles and prevent the fusing of these particles together, hence inhibiting the sintering process in the affected regions. In this paper the factors affecting the SIS-Metal process based on microscopic mechanical inhibition is investigated. By the aid of response surface methodology the effective factors have been evaluated to improve the part strength, surface quality and dimensional accuracy produced by the SIS-Metal process.*

Keywords: *Metallic parts fabrication; Powder sintering; Selective inhibition; Rapid prototypes; Design of experiments; Regression; Optimization; desirability function.*

1. INTRODUCTION

The Selective Inhibition Sintering (SIS) process is an additive manufacturing (AM) technology which builds parts on a layer-by-layer basis. The principle idea of the SIS process is the prevention of selected segments of each powder layer from sintering. Therefore, the SIS process may be considered as an opposite approach to the Selective Laser Sintering (SLS) process in which selected areas of powder are sintered by a fine laser beam. In previous work on the SIS for polymer powder [Khoshnevis *et al*, 2010] it was demonstrated that the SIS based on Microscopic mechanical inhibition for metal process can fabricate parts at a high speed

using relatively low cost machines. In the research here the factors affecting the SIS process for metallic parts based on microscopic mechanical inhibition will be evaluated and improved. Response surface methodology techniques are used for identifying the effective factors that affect the part quality. Optimization is then used to determine the desirable values of the related variables.

2. SIS METAL PROCESS BASED ON MICROSCOPIC MECHANICAL INHIBITION

The SIS-Metal process based on *microscopic mechanical inhibition* is shown in Figure 1. Compared to the layer-by-layer sintering

approach used in the SIS-Polymer process, a bulk sintering approach is adopted for SIS-Metal. This is mainly due to a longer cycle time that is required in heating and cooling metal powder compared to plastic powder. In addition, the layer-by-layer sintering of metal powder would require the fabrication machine to operate in an oxygen-free environment. Hence, the required hardware would be cost prohibitive. Finally, undesirable shrinkage effect among sintered layers may be generated in the layer-by-layer sintering approach, which would create undesired internal stresses.

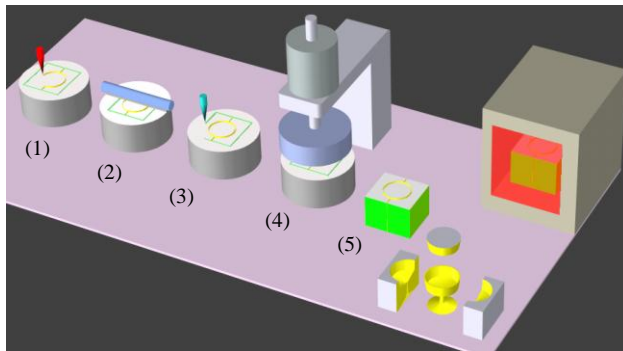


Figure 1: The SIS-Metal process based on the microscopic mechanical inhibition

The SIS-Metal process based on the bulk sintering approach has five main steps as follows:

- (1) **Printing sintering inhibitor:** A deposition nozzle with a fine orifice, or an inkjet print head, is used to deliver a sintering inhibitor to the selected areas (i.e., layer profile) of the powder layer. If aqueous solutions are used, the layer is dried before continuing with the subsequent layer.
- (2) **Laying a thin powder layer:** Metal powder is spread as a thin layer over the build tank using a blade or a roller.
- (3) **Creation of a boundary to contain part:** A consolidating liquid is deposited on the powder bed at the periphery of the part profile. The profile of this deposition may be a simple shape such as square or circle. When all the layers are completed, such depositions will create a solid container

around the area that includes the 3D part. Using this container the completed green part can then be removed from the machine and transferred to the sintering furnace. Interestingly, the salt solution used as the printed inhibitor can hold the metal powder particles together after it is dried. The consolidating liquid for creating the container can be different from the inhibitor solution, however.

- (4) **Heating and compression:** A heater is used to evaporate water and other liquid additives (such as alcohol which may be needed for breaking surface tension) in the printed inhibition sections. An optional motorized press may be used to compact the metal powder layer after drying the inhibitor solution in order to create a powder bed with increased density. Although layer compression can improve part density, it may also result in part deformation. Successful implementation of compression requires careful study of the deformation process so that the effect may be properly incorporated in the CAD model. The layer compression was not performed in the study presented in this paper.
- (5) **Bulk sintering in an oven:** After all the layers have been completed, a metal powder block is extracted from the build tank and placed in a conventional sintering oven. A high temperature ceramic base plate, initially placed on the build tank piston may be used for picking up the unsintered loose powder block. After sintering and cooling, the sintered metal block is removed from the oven. Finally, the fabricated part can be extracted by removing the regions that are isolated by the inhibited powder areas.

3. ADVANTAGE OF SIS METAL

Currently, many AM processes have been developed for building metallic parts, such as Selective Laser Sintering (SLS), 3D Printing (3DP), Fused Deposition Modeling (FDM),

Direct Metal Laser Sintering (DMLS), Laser Engineered Net Shaping (LENS), and Electric Beam Melting (EBM). These processes can be classified based on the usage of binders and the sintering approach as shown in Figure 2.

- Usage of binders:** Some AM processes such as SLS, 3DP, and FDM utilize certain binders in the fabrication of green parts. For example, the SLS process uses polymer-coated metal powder [Wohlert, *et al.* 1996; Pease 1998]; the 3DP process deposits droplets of liquid acrylic copolymer binder onto a bed of metal powder [Sachs, *et al.*, 2000; Pease 1998]; and the FDM process uses filaments that are made by a mixture of binder and metal powder [Greul *et al.* 1995]. The binders in the fabricated green parts can then be removed in a thermal debinding step. In comparison, AM processes such as DMLS, LENS, and EBM can directly sinter metal powders layer-by-layer using high-power energy sources. For example, the DMLS process can directly sinter metal powder without using polymer coating [Simchi, *et al.* 2001; Kotila, *et al.* 2001; Behrendt and Shellabear, 1995]. The LENS process directly produces metal parts from metal powder injected by a powder delivery nozzle [Atwood, *et al.* 1998]. The EBM process can also directly melt metal powder in a controlled atmosphere chamber using an electron beam.
- Sintering approach:** Based on how metal powders are sintered into finished metallic parts, AM processes can also be classified into bulk sintering and layer sintering. In the AM processes based on bulk sintering of metal powders (e.g. SLS, 3DP, and FDM), green parts are fabricated first and are then transferred to a sintering oven. In comparison, in the AM

processes based on layer sintering of metal powders (e.g. DMLS, LENS, and EBM), powders are sintered into the predefined geometry layer by layer. As discussed before, bulk sintering can have advantages such as lower hardware cost, reduced deformation and higher building speed.

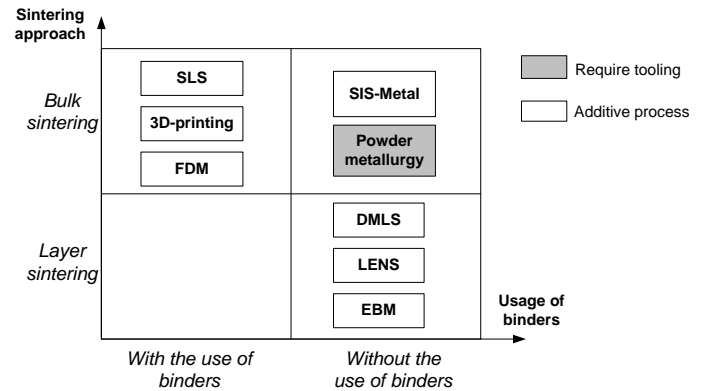


Figure 2: A classification of the metallic part fabrication processes

Based on such a classification the SIS-Metal process is uniquely positioned among all the metallic part fabrication processes because it is a layered fabrication process which is based on the bulk sintering approach without using any binder. As shown in Figure 3, the SIS-Metal process is classified in the same category as the traditional powder metallurgy process. However, as no tools are required, the SIS-Metal process may be regarded as a moldless powder metallurgy process.

The SIS-Metal process has the following advantages.

- The hardware of the SIS-Metal process can be inexpensive. A green part can be fabricated using a print head to deposit the inhibitor solution to powder layers; the green parts can then be sintered in a conventional sintering oven, which is widely available in a typical powder metallurgy manufacturing facility.
- The SIS-Metal process is potentially fast. The inhibitor can be deposited using a multi-jet print head, which has proven performance and impressive speed in other applications such as two-dimensional (2D) printing. The printing time can be further reduced using a vector (instead of a raster) printer, because in most cases the inhibitor needs to be deposited as a thin line only along the boundary of each layer profile.
- The SIS-Metal process can have less shrinkage and deformation since no de-binding is involved.
- Unlike LENS or DMLS, no complex supports are required in the SIS-Metal process since overhang features are supported by powder volumes underneath.

Consequently, the development of the SIS-Metal process is important for future metallic part fabrication.

4. EXPERIMENTAL PROCEDURE

A three-axis prototype machine has been developed as shown in Figure 3. In the machine a single print nozzle with an orifice size of 0.005" (0.127 mm) is used. The large orifice size of the nozzle allows the trial of different inhibitors at different viscosity levels. The printing nozzle used has an electro-magnetic solenoid valve for droplet printing. The deposited droplets are 300 nanoliters in volume and are dispensed at the frequency of 1500 HZ. Changing the nozzle frequency changes the droplet size. The voltage that controls the solenoid valve is

another factor that affects the droplets size. The nozzle moves in the X and Y axes by stepper motors with a continuous speed of 31 mm/second. A heater has been incorporated for heating up every layer after printing the inhibitor. The heater can heat up every layer up to 200°C to evaporate the liquid in the inhibitor solution. Heating temperature and heating time are other factors that impact the final part dimensional accuracy.

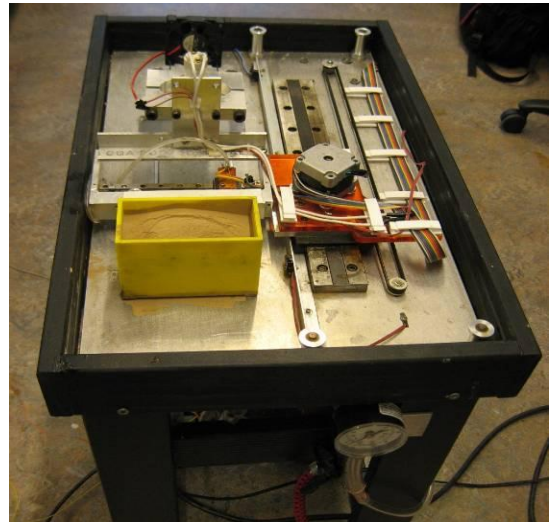


Figure 3: The SIS prototype machine

Metal powder: Bronze powder has been the choice of metal powder in this research because of its relative ease of sintering and because of the popularity of bronze parts. Mixed, partially alloyed and fully alloyed bronze powders have been investigated for use in this research project. Sintered parts with fully alloyed bronze powders showed the best mechanical properties and the least shrinkage. In addition to copper (about 90%), the bronze powder used in our experiments has the following chemical compositions:

Tin:	10%
Lead:	0.025%
Zinc:	0.04%
Iron:	0.058%
Phosphorous:	0.085%

Metal powders with different mesh sizes and shapes have also been examined. The finer the grain size, the better the sintering process will be. However, if the grain size is too small it would be difficult to spread the powder as a uniform layer. The most suitable grain size was observed to be 325 meshes or 44 micron. The shape of metal powder is another important factor. The density of green parts is directly related to the packing density of the powder bed. The packing density of spherical powder is better than other shapes. Therefore, spherical fully alloyed bronze powder with 44 micron grain size was used in this study. The powder particle size has the following distribution:

325 Mesh (44 Micron)	98.7 %
200/325 Mesh (44/75 Micron)	1.3 %

4.1 Inhibitor

In our study, salts have been chosen as the best inhibitor candidates, since salts are usually inexpensive and safe for both human and environment. Salt crystals can be easily and quickly formed from the printable salt solution state. The following important factors need to be considered in choosing an appropriate salt candidate: (1) the initial salt crystal size must be significantly smaller than the size that is yielded under early sintering temperature of about 170-200 °C; (2) molecular mass of the salt solution and its surface tension should be small such that it can have sufficient penetration in metal powder; and (3) The salt solution should have a high solubility for nucleating a higher amount of crystals from a droplet.

Molecular formula	$\text{Al}_2(\text{SO}_4)_3$
Molar mass	342.15 g/mol (anhydrous)
Melting point	770 °C
Solubility in water	36.4 g/100 mL (20 °C) 89.0 g/100 mL (100 °C)

Solubility in alcohol and acids	slightly soluble in alcohol and dilute mineral acids
---------------------------------	--

Table 1: Properties of aluminum sulfate

Accordingly, the best inhibitor was identified to be aluminum sulfate. The properties of aluminum sulfate are shown in Table 1. The inhibitor is achieved by solving 32 grams of aluminum sulfate anhydrous in 130 ML of water at room temperature with 30 ML of isopropyl alcohol. Isopropyl alcohol is added to the inhibitor in order to break the surface tension of the solution so that the inhibitor can easily penetrate the printed sections.

4.2 Green part fabrication procedure

The 3-Dimensional CAD model of the part to be built is first sliced into a set of layers with equal thickness. Depending on the part geometry, the layer thickness in our tests varied from 0.25 mm to 1 mm. For every layer the platform of the SIS prototype machine goes down a layer thickness to accommodate the powder for the next layer to be built. After the metal powder is spread the print nozzle, which can move along both X and Y axes, prints the inhibitor on the sections to be prevented from bonding by sintering. The inhibitor is also printed on the boundary of the part to create a solid container around the area that contains the 3D part. It is with this container that the green part is picked and placed in the sintering furnace. After inhibitor printing is completed for every layer the heater heats up the layer to dry up the inhibitor solution. As shown in Figure 2, the process then repeats for other layers. After all layers are created the fabricated green part is transferred to a sintering furnace. The sintering path in the oven is discussed as follows.

4.3 Sintering path

The sintering happens in an inert environment with Argon gas. Various sintering paths have

been tested. A sample sintering path that yields reasonably small shrinkage is shown in Figure 4

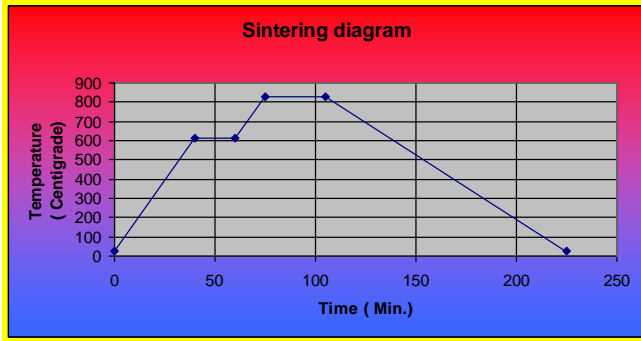


Figure 4: Desired sintering path used in the experiments

The next step is to build 3-D models and use DOE to improve the property. After designing the 3-D model shown in Figure 5 the model is sliced using a slicing program. The SIS machine tool path follows the boundary points for every slice and prints the inhibitor on the printed sections. The tool path for every slice and the printed sections for every slice are shown in figure 6.

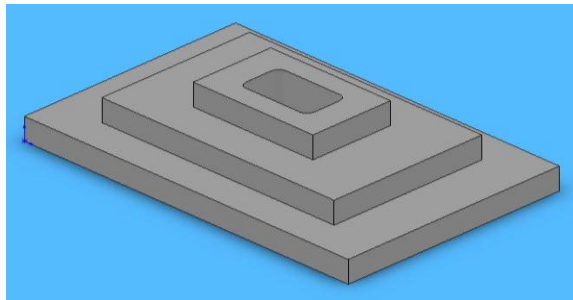


Figure 5: 3-D model designed in solid works for being built by the SIS machine

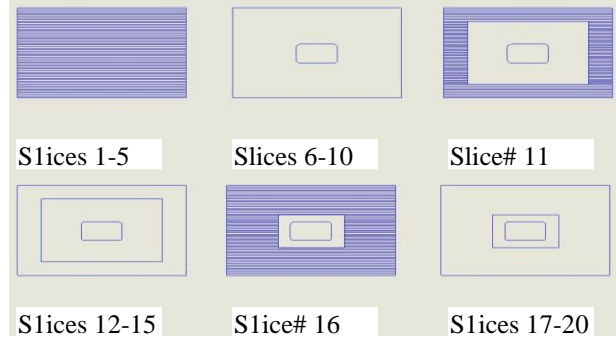


Figure 6: Printed sections for every slice

4.4 Preliminary Experimental results

Two of fully sintered bronze parts made are shown in Figures 7. Note that the print nozzle used in our testbed has a low resolution (~0.13 mm). As illustrated by other commercial processes such as 3DP, improving the nozzle resolution can lead to drastically better surface quality.

The properties of the bronze part shown in Figure 7 have been determined and listed tested in Table 2.

Linear shrinkage	8%
Hardness (BHN)	60
Ultimate Tensile Strength	30,000 psi
Density	6.8 gr/cm ³

Table 2: Mechanical properties of a bronze part build by the SIS process

Various tests have been performed in this research in order to understand the inhibition mechanism in the presence of printed salt in metal powder. A scanning electron microscope (SEM) is used to examine the interactions between metal powder particles and salt crystals in the SIS-Metal process. The SEM pictures of the bronze powder with and without salt, and also before and after sintering are shown in Figure 9.

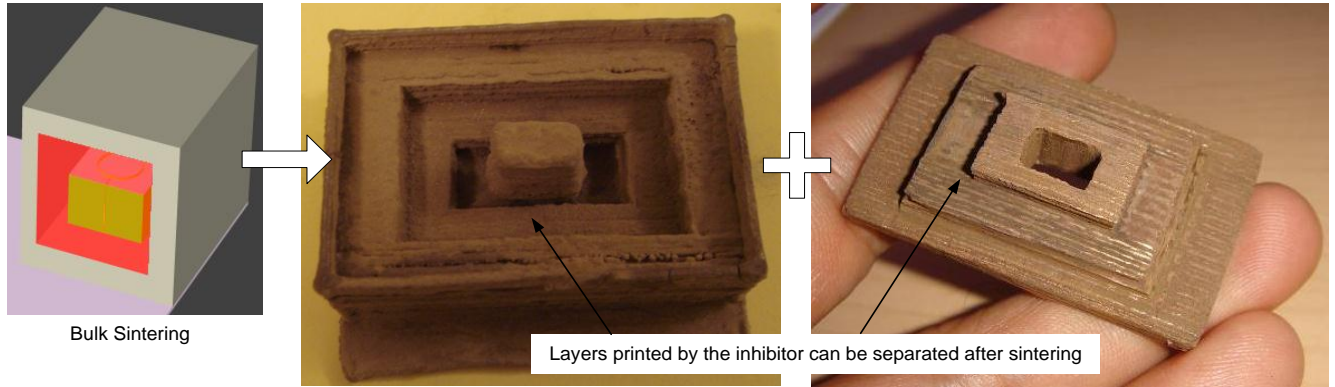


Figure 7: A test bronze part can be separated from other portions after sintering

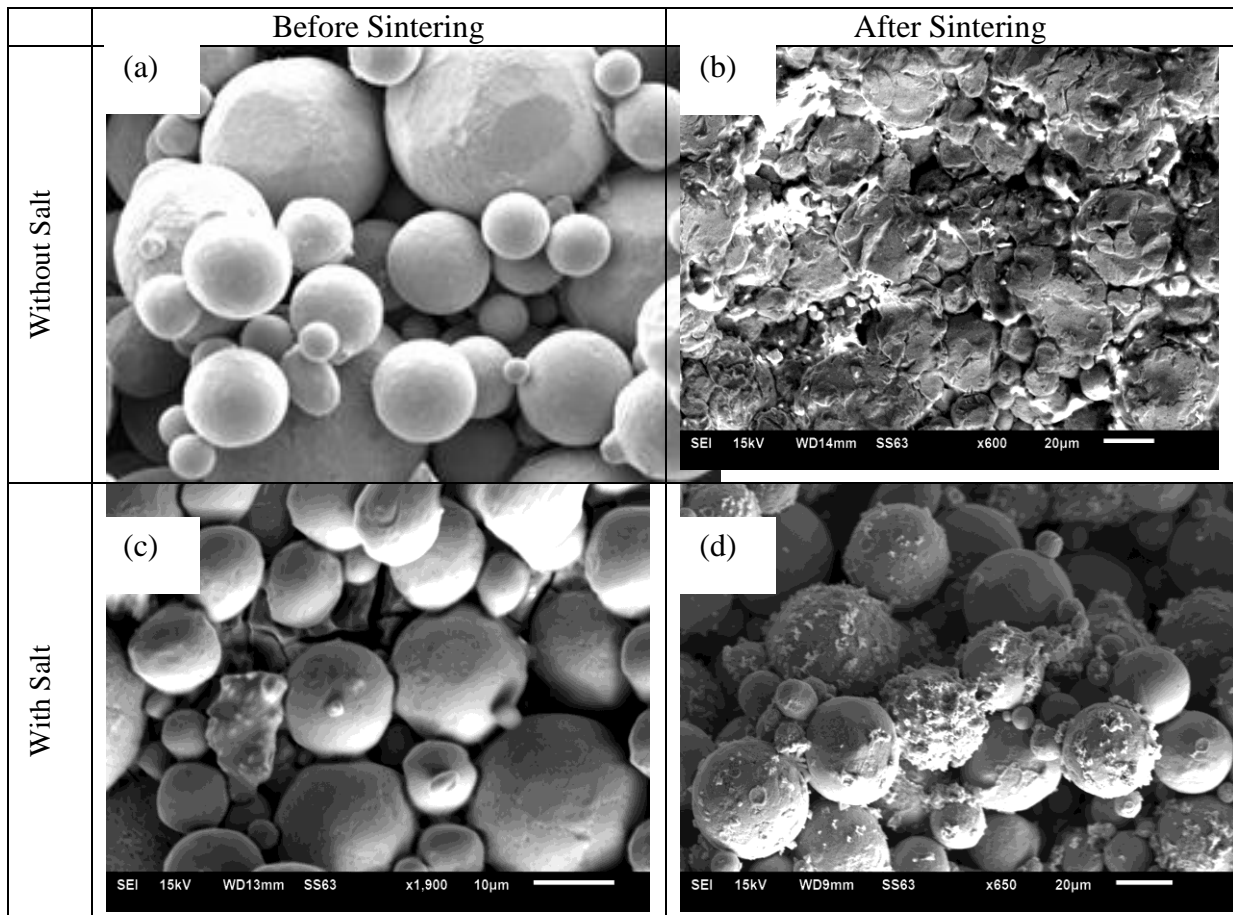
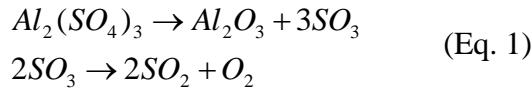


Figure 8: The SEM pictures of different samples. (a): a sample that is unsintered and without salt; (b): a sample that is sintered and without salt; (c): salt crystals are embedded in a sample that is unsintered and with salt; (d): metal powder particles are covered by ceramic particles and other substances in a sample that is sintered and with salt

The decomposition of aluminum sulfate during the sintering process is shown as follows:



As noted before, aluminum sulfate starts decomposing at 500 °C and fully decomposes at around 800 °C. Another property of aluminum sulfate which becomes important here is that its melting point is around 760 °C. Therefore, when the furnace temperature is over the melting point of aluminum sulfate the remaining non-decomposed salt crystals melt before they fully decompose to aluminum oxide. Hence, molten salt uniformly coats some adjacent metal particles. As the temperature raises this salt coating decomposes into aluminum oxide which gives a near-perfect ceramic coating to the affected metal particles. A sample particle which has been subject to such ceramic coating is shown in figure 9.

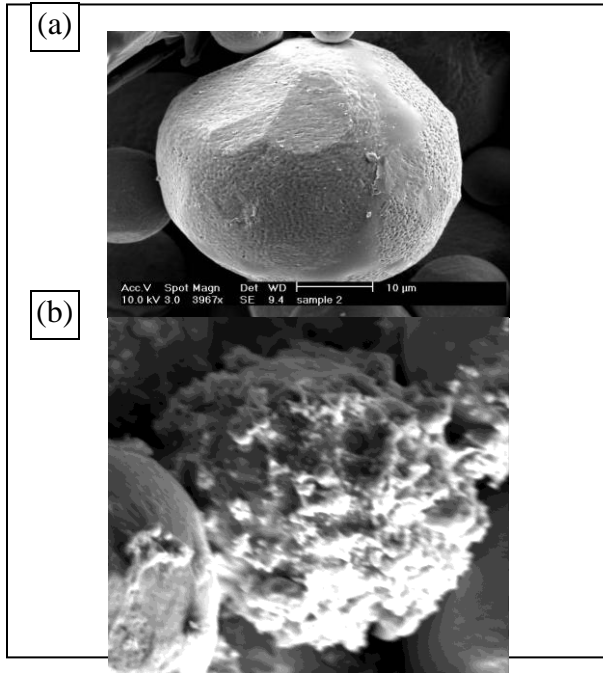


Figure 9: The SEM pictures of different samples: (a): a metal powder particle before sintering; (b): a metal powder particle that is coated with ceramic

5. DOE FOR SURFACE SMOOTHNESS AND DIMENSIONAL ACCURACY

For surface smoothness and dimensional accuracy the effective factors based on our preliminary results are the following:

- 1- Frequency of the solenoid valve used for printing
- 2- Voltage of the solenoid valve used for printing
- 3- Layer thickness
- 4- Heating temperature for inhibitor fluid evaporation
- 5- Heating time

We decided to run a 2^{5-1}_v plus a 3 center points (using $X5=X1*X2*X3*X4$ as the generator). This yields a total of 19 runs. We believe there are probably some two factor interactions plus a chance of curvature for some or all factors. Also, we know that in a 2^{5-1}_v plan all main effects are alias with 4 factor interactions and two factor interactions are aliased with three factor interactions. So, we are able to estimate all main effects and two factor interactions. The coded and natural parameters based on current operational points are as follow:

		-1	0	1
X1	Frequency (Hz.)	1350	1500	1650
X2	Voltage	4.5	7	9.5
X3	Layer thickness	240 (1mm)	275 (2mm)	310 (3mm)
X4*	Heating temperature(Celsius)	140	160	180
X5	Heating time(min.)	2	3	4

Table 3: Factor levels for dimensional accuracy

After running all settings the two responses were measured as the representative quality of produced parts.

- 1- Surface smoothness
- 2- Corner sharpness

We assigned a number to the set of {2, 4, 6, 8, 10}, while 2 represents the worst quality and 10 represents the highest quality. The data for

all 19 settings and their responses are shown in Table 4.

	X1	X2	X3	X4	X5	Corners	Surface
1	-1	-1	-1	1	-1	6	10
2	-1	1	1	1	-1	8	6
3	-1	1	-1	-1	-1	6	8
4	-1	1	-1	1	1	8	8
5	1	-1	1	-1	1	8	6
6	1	1	1	1	1	4	10
7	1	1	-1	1	-1	4	8
8	1	-1	-1	1	1	2	8
9	-1	-1	1	1	1	8	10
10	0	0	0	0	0	6	6
11	-1	-1	1	-1	-1	4	4
12	1	-1	1	1	-1	10	8
13	-1	-1	-1	-1	1	2	4
14	0	0	0	0	0	4	8
15	0	0	0	0	0	6	8
16	1	1	1	-1	-1	10	10
17	1	-1	-1	-1	-1	6	8
18	1	1	-1	-1	1	2	4
19	-1	1	1	-1	1	10	6

Table 4: Design table for dimensional accuracy and surface smoothness

Source	DF	Sum of Squares	Mean Square	F Ratio
Model	16	125.33	7.83	5.88
Error	2	2.67	1.33	Prob > F
C. Total	18	128.00		0.16

Table 5: Analysis of Variance for surface smoothness

Source	DF	Sum of Squares	Mean Square	F Ratio
Model	16	69.75	4.36	3.27
Error	2	2.67	1.33	Prob > F
C. Total	18	72.42		0.26

Table 6: Analysis of Variance corners' sharpness

Running the JMP Statistical Analysis software gives interesting results. In fact, for two reasons the results were not quite acceptable for us:

- 1- We already know that most parameters have significant impacts on the results, but in this analysis most of them are shown as being insignificant.
- 2- We also know that there are many noises that are imposed by our imprecise prototype machine and such noises have to be considered in this investigation.

With those concerns in mind and our experiences with this technology as well as the results of this analysis we increased the alpha level, because a) our goal is improvement not optimization, and b) we have a chance to test the analysis results and verify it. Accordingly, the regression equations became as follow:

$$\text{Smoothness} = 6 + 1.625X_3 - 1.125X_1X_2 - 1.125X_1X_5 - 0.875X_1X_4 - 0.375X_1 \quad (\text{Eq. 2})$$

$$\text{Corners} = 7.368 + 1.125X_4 + 0.875X_3X_5 + 0.875X_4X_5 - 0.375X_5 \quad (\text{Eq. 3})$$

Both equations 2 & 3 are in coded variables.

5.1 Desirability

There are two different equations (surface smoothness and corners' sharpness) with two different goals in this analysis. The method presented by Myer and Montgomery is used here to optimize the combined effect of the criteria represented by these equations. First we define $d(s)_i$ for i^{th} setting as follow:

Source	DF	Sum of Squares	Mean Square	F Ratio
Model	15	0.11742725	0.007828	11.9831
Error	3	0.00195988	0.000653	Prob > F
C. Total	18	0.11938714		0.0320*

Table 7: Analysis of Variance for response D

Source	DF	Sum of Squares	Mean Square	F Ratio
Lack Of Fit	1	0.00051786	0.000518	0.7182
Pure Error	2	0.00144202	0.000721	Prob > F
Total Error	3	0.00195988		0.4860
Max Rsq	0.9879			

Table8: Lack of fit for response D

$$d(\text{smooth})_i = (\text{Smooth}-0) / (30-0) = \text{Smooth}/30 \quad (\text{Eq. 4})$$

In the above equation, 0 is the minimum acceptable and 30 is the ideal amount of smoothness. Also, note that if $d(\text{smooth})_i < 0$ then we consider that as 0 and if $d(\text{smooth})_i > 1$ we consider that as 1. By the same token for corner sharpness we have:

$$d(\text{corner})_i = (\text{corner}-0) / (20-0) = \text{corner}/20 \quad (\text{Eq.5})$$

In the above equation 0 is the minimum acceptable sharpness and 20 is the maximum corner sharpness or the ideal sharpness for this technology.

Then D_i can be calculated for the i^{th} setting as follow:

$$D_i = (d(\text{smooth})_i * d(\text{corner})_i)^{1/2} \quad (\text{Eq. 6})$$

We used the JMP software to analyze the settings with the new response (D_i).

Significant factors defined the relationship between D and the process parameters as follow:

$$D = 0.264967 + 0.0380166X_3 - 0.0341X_1 * X_5 - 0.0303 X_1 * X_4 + 0.0272192 X_1 * X_3 + 0.0246809 X_3 * X_5 - 0.024349X_2 * X_4 - 0.024321 X_5 + 0.0213225 X_4 - 0.020603 X_1 * X_2 \quad (\text{Eq. 7})$$

This is of course a relatively complicated relation. In fact, different interactions make many distortions in the shape of the response surface.

	Natural					D (Predict)	smooth (Predict)	Corners (Predict)
	X1	X2	X3	X4	X5			
Base	1500	7	275	160	3			
Delta	-15.2065	0	35	11.21747	0.6397			
1/2 Delta	-7.60326	0	17.5	5.608734	0.3199			
1/2 Delta(Corrected)	-10	0	17.5	5	-0.3			
Base+1/2delta	1490	7	292.5	165	2.7	0.29207	6.815	7.56488
Base+ delta	1480	7	310	170	2.4	0.30961	7.585	7.368
Base+ 1.5 delta	1470	7	327.5	175	2.1	0.31757	8.31	6.77738
Base+ 2 delta	1460	7	345	180	1.8	0.31595	8.99	5.793

Table 9: Optimization for D using steepest ascent method

Following are some remarks about Table 9:

- 1- After calculating “Delta” we were forewarned by our experience that 35 units in layer thickness is an unduly large, therefore, we decided to try one half of “Delta”.
- 2- Also we noticed implementing the exact amounts of increase or decrease on each parameter would be impossible because of the precision limitations. Accordingly, we decided to round up the related quantities to more reasonable and practicable values.
- 3- We limited the green part heating temperature to 180 C, which is the maximum that our current heater hardware allows.
- 4- Although it was observed that D increased at each step, after 4 runs corner sharpness started to deteriorate, therefore, higher values were not tried.

5.2 Validation

After running the first 4 runs it was noticed that the second setting yielded the best outcome. This setting was run two more times and consistently yielded the same result. Therefore this setting was picked as the best.

Factor	Value
Frequency	1480 HZ
Voltage	7 volts
Layer thickness	310 (3 mm)
Heating temperature	170 Celsius
Heating time	2.4 min.

Table 10: Optimal points for dimensional accuracy and surface smoothness

Theoretically, we could continue from this point by introducing a central composite design. But we stop here due to the limitations of our machine. In other words, with a higher quality machine, which has a more precise printing capability, significantly better parts can be produced as the result of an extended experimentation. Furthermore, the result of this study also has one clear message: the SIS technology is a promising method for rapid fabrication of free form metallic parts.

6. DOE FOR SHRINKAGE & HARDNESS

In order to improve the parts in the course of our preliminary results we used the Response

Surface Methodology (RSM). The software tools chosen for implementing RSM are Minitab and JMP. The first part of DOE was to improve the shrinkage and the hardness of the specimens. Several parts were made in order to find the effective parameters which could improve the hardness and shrinkage of the final parts. The four effective parameters are listed below and characterized in Table 11:

	-1	0	1
T1(°c)	600	615	630
t1(Sec.)	10	15	20
T2(°c)	810	820	830
t2(Sec.)	25	30	35

Table 11: Coded values for design parameters T1, T2, t1 and t2

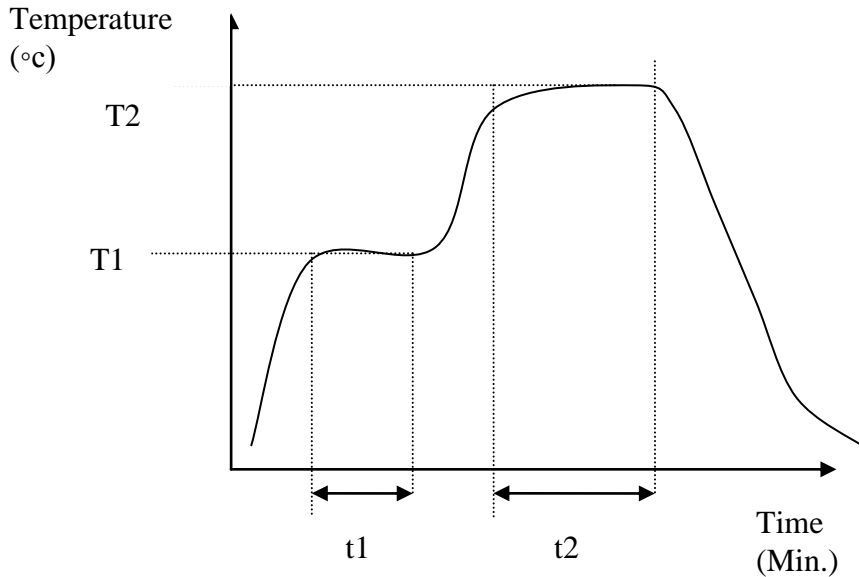


Figure 10: Sintering path showing Temperature Vs. Time

T1: temperature of the first step sintering,
 t1: time during first stage of sintering
 T2: temperature of the first step sintering,
 t2: time during first stage of sintering

Temp1	Time1	Temp2	Time2	Hardness(BN)	Shrinkage %
-1	1	1	-1	82	0.088126
-1	-1	1	1	76	0.131762
1	-1	1	-1	57	0.112101
...
.

Table 12: Full factorial design 4 design parameters T1, T2, t1 and t2 with response Hardness and shrinkage percentage

The same approach is used for improving the dimensional accuracy is used here too. After running the experiments in the furnace using all these 16 parameters with 4 center points and feeding the results to JMP the following were concluded:

$$\text{Hardness (Brinell)} = 65.275 - 1.688 T_1 + 2.063 T_2 + 0.563 t_2 + 2.313 T_1 * t_1 - 2.438 t_1 * t_2 - 2.5 T_2 * t_2 \quad (\text{Eq. 8})$$

$$\text{Shrinkage (percentage)} = 0.108 - 0.004 t_1 + 0.003 T_2 + 0.011 t_2 + 0.006 T_1 * t_1 + 0.003 T_1 * T_2 \quad (\text{Eq. 9})$$

All concerns regarding noises and goal of experiments present in the printing section stood valid here as well. The two different equations (Hardness and shrinkage) have two different goals. To combine those goals in a unique criterion and optimize it we use the Myer and Montgomery method by first defining the $d(s)_i$ and $d(h)_i$ for i^{th} setting as follow:

$$d(s)_i = (0.25 - S) / (0.25 - 0.05) = (0.25 - S) / 0.2 \quad (\text{Eq. 10})$$

In the above equation 0.25 is the maximum shrinkage acceptable and 0.05 is the ideal

amount. S is the amount of shrinkage in each setting. Also, note that if $d(s)_i < 0$ then we consider it to be 0 and if $d(s)_i > 1$ we consider it to be 1. We have,

$$d(h)_i = (H - 40) / (120 - 40) = (H - 40) / 80 \quad (\text{Eq. 11})$$

In the above equation, 120 is the maximum Hardness and 40 is the ideal amount. S is the amount of shrinkage in each setting. Also note that if $d(h)_i < 0$ then we consider it to be 0 and if $d(h)_i > 1$ we consider it to be 1. D_i for i^{th} setting can be calculated as follow:

$$D_i = (d(s)_i \times d(h)_i)^{1/2} \quad (\text{Eq. 12})$$

Analyzing the data yielded the following regression for D:

$$D = 0.462368 - 0.027496 T_2 * t_2 - 0.024205 t_1 * t_2 + 0.0169568 T_1 * t_1 - 0.014725 T_1 - 0.013062 t_2 + 0.0128973 T_2 \quad (\text{Eq. 13})$$

Now we use the steepest ascent method to find the optimal point, as shown in Table 13.

	Natural				D (predicted)	Shrinkage (Predicted)	H (Predicted)
	Temp1	Time1	Temp2	Time2			
Base	615	15	820	30			
Delta	8.03299	0	2.345305	4.750509165			
Delta (corrected)	-8	0	2	-5			
Base+ delta	607	15	822	25	0.4874105	0.10306	67.22196667
Base+ 2 delta	599	15	824	20	0.5234513	0.09684	70.16593333
Base+ 3 delta	591	15	826	15	0.5704906	0.08934	74.1099
Base+ 4 delta	583	15	828	10	0.6285282	0.08056	79.05386667
Base+ 5 delta	575	15	830	5	0.6975643	0.0705	84.99783333
Base+ 6 delta	567	15	832	0	0.7775987	0.05916	91.9418

Table 13: Optimization for D using steepest ascent method

In table 13 in the fourth run the results began showing relatively large differences with predicted values. This is mostly because

reducing time in the second phase led us to a part that was not sintered well. The best setting in this study is shown in Table 14.

T1: Temperature of the first step sintering	591
t1: Time during first stage of sintering	15
T2: Temperature of the first step sintering	826
t2: Time during first stage of sintering	15

Table 14: Optimal settings for maximum hardness and minimum shrinkage

7. IMPROVING THE SIS PARTS

As may be seen in Figure 11 there is a big improvement in the dimensional accuracy and surface smoothness in the printed layers by implementing the new settings identified by the DOE results. In figure 11 printed layers in the preliminary experimental stage prior to the improvement are shown in the left and printed layers with the new setting to improve surface smoothness and dimensional accuracy are shown in right .The parts dimensional accuracy is improved by 10% in precision. The final part hardness is 70 and the linear

The predicted value for the optimal linear shrinkage for the setting shown in table 14 is 8% and the optimal hardness is 75 BHN. shrinkage is 8%, which is close to the value predicted by the DOE results.

8. CONCLUSION

Factors affecting the dimensional accuracy, surface smoothness, part strength and shrinkage of the parts fabricated by the SIS process for metallic parts based on microscopic mechanical inhibition have been identified. Upon identifying these factors the DOE method and optimization techniques have been used to improve the final parts. The new settings improved the experimental process of fabricating the final parts. By establishing the basic process and mechanism we expect the SIS-Metal process to be further improved by investigating alternative powder materials and inhibitors, finer printing nozzle, and other relevant factors.

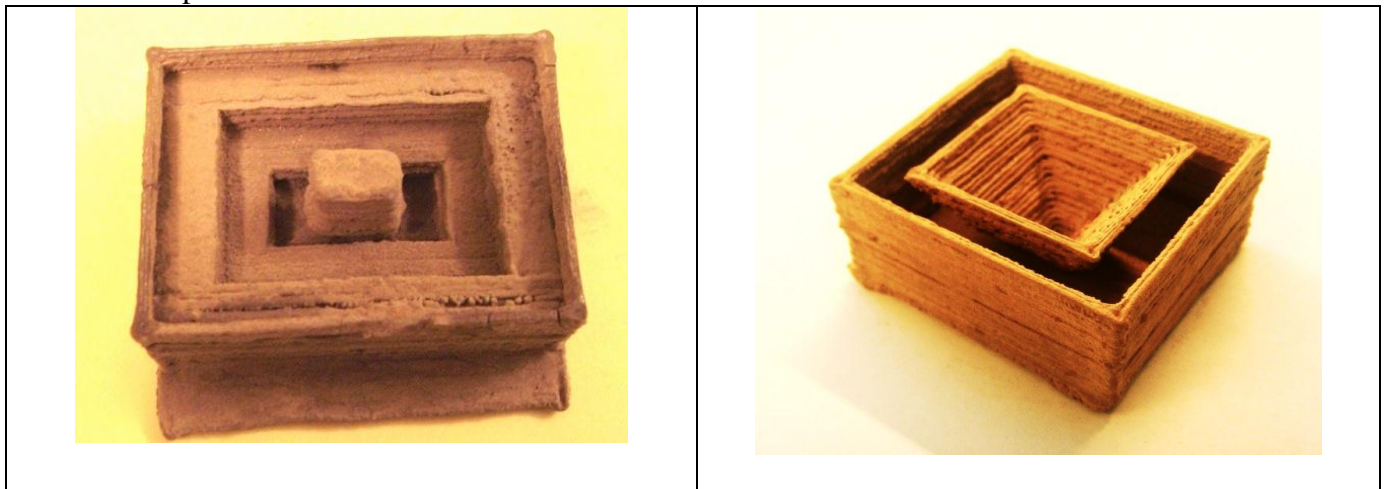


Figure 11: Two different printed layers by the SIS process

REFERENCES

- [1]Apte, N. G., Kiran, E., and Hassler, J.C. (1988), “ Kinetic modeling of thermal decomposition of aluminum sulfate”, *Chem Eng. Comm*, Vol. 74, pp 47-61.
- [2]Asiabanpour, B., Palmer, K. and Khoshnevis, B. (2004), “An experimental study of surface quality and dimensional accuracy for selective inhibition of sintering”, *Rapid Prototyping Journal*, Vol. 10 No. 3, pp. 181-92.
- [3]Asiabanpour, B., Khoshnevis, B. and Palmer, K. (2006), “Advancements in the selective inhibition sintering process development”, *Virtual and Physical Prototyping Journal*, Vol. 1 No. 1, pp. 43-52.
- [4]Atwood, C., Griffith M., Harwell L., Schlienger E., Ensz M., Smugeresky J., Romero T., Greene D., and Reckaway D. (1998), “Laser engineered net shaping (LENS): a tool for direct fabrication of metal parts,” Sandia National Labs, http://mfgshop.sandia.gov/1400_ext/icaleo98.pdf.
- [5]Behrendt, U., and Shellabear M. (1995), “The EOS Rapid Prototyping Concept,” *Computers in Industry*, Vol. 28.
- [6]German, R.M. (1994), *Powder metallurgy science*, 2nd ed., Metal Powder Industries Federation, Princeton.
- [7]Greul, M., Pintat T., and Greulich M. (1995), “Rapid prototyping of functional metallic Parts”, *Computers in Industry*, Vol. 28, No. 1, pp. 23-28.
- [8]Kalpakjian, S., and Schmid, S. (2006), *Manufacturing Engineering and Technology*, Pearson Prentice Hall, 5th edition.
- [9]Khoshnevis, B., Asiabanpour B., Mojdeh M., and Palmer K. (2003), “SIS – a new SFF method based on powder sintering”, *Rapid Prototyping Journal*, Vol. 9, No. 1, pp. 30-36.
- [10]Kotila, J., Nyrhilä O., and Syvänen T. (2001), “Direct steel component manufacturing using direct metal laser sintering”, *Advances in Powder Metallurgy & Particulate Materials – 2001*, MPIF, Princeton, U.S.A.
- [11]Pease L. F. (1998), “Selective laser sintering,” *ASM Handbook Volume 7: Powder Metal Technologies and Applications*.
- [12]Pelovski, Y., Pietkova, W., Grunchov, I., Pacewska, B. and Pysiak, J. (1992), “ The thermal decomposition of aluminum sulfate in different gas phase environments” *Thermochemica Acta*, Vol. 205, pp.219-224.
- [13]Sachs, E., Allen S., Cima M., Brancazio D., Serdy J., Polito B., Ables D., and Rynerson M. (2000), “Three dimensional printing: a candidate for the production of powder metal parts,” *Advances in Powder Metallurgy and Particulate Materials*, Vol. 1, pp. 139-152.
- [14]Simchi, A., Petzoldt F., and Pohl H., (2001) “Direct metal laser sintering: material consideration and mechanisms of particle bonding,” *The International Journal of Powder Metallurgy*, vol. 37, n. 2.
- [15]Smith, R. L. and Yanina S. V. (2002), “Inhibition of sintering and surface area loss in phosphorus-doped corundum derived from diasporite”, *Journal of Am. Ceram. Soc.*, Vol. 85, No. 9, pp. 2325-30.
- [16]Stern, K. H., (2001), *High temperature properties and thermal decomposition of inorganic salts with oxyanions*, CRC Press, Ltd, pp. 74-75.
- [17]Stuecker, J., Cesarano J., and Hirschfeld D. (2003), “Control of the viscous behavior of highly concentrated mullite suspensions for robocasting”, *Journal of Materials Processing Technology*, Vol. 142, No. 2, pp. 318-325.
- [18]Tagawa, H. (1984), “Thermal decomposition temperatures of metal sulfates”, *Thermochemica Acta*, Vol.80, pp. 23-33.
- [19]Wohlert, M., Bourell D., Lee G., and Beaman J. (1996), “Production of full density metal-matrix composite by a combined

selective laser sintering/metal infiltration process,” Processing and Fabrication of Advanced Materials V, The Minerals, Metals & Materials Society.

[20] Myers R, Montgomery D. *Response Surface Methodology* (2nd edn). Wiley: New York, 200

BIOGRAPHIES

Mahdi Yoozbashizadeh is a graduate research assistant and a PhD candidate at University of Southern California in the field of manufacturing engineering. His back ground is in mechanical engineering design and manufacturing. Currently his research is focused on rapid prototype systems. More information can be found on his homepage: <http://www-scf.usc.edu/~yoozbash/>

Dr. Khoshnevis is a Professor of Industrial & Systems Engineering, Aerospace & Mechanical Engineering, and Civil and Environmental Engineering at USC. He has extensive experience in invention and commercialization of products

and processes and has numerous innovations in diverse fields ranging from medical devices to oil and gas and construction fields. His inventions, especially in robotics construction, have received worldwide coverage in acclaimed media.

Nozar Mozaka earned his Bachelor degree in Industrial Engineering from Isfahan University of Technology (IUT) in 1994 and his Master in Industrial Engineering from Tehran University in 1996. He worked in Iran for 10 years including 5 years at IKCO (A big car maker) in quality field. In 2006 he immigrated to the U.S. and started working at Pacific Sintered Metals (PSM) as a Quality Engineer. He earned his second Masters degree in Manufacturing Engineering from University of Southern California (USC) in 2010. He is currently working at JE Pistons as a Quality Engineer.